Materials Research Express

PAPER

Acid hydrogel matrixes as reducing/stabilizing agent for the in-situ synthesis of Ag-nanocomposites by UV irradiation: pH effect

Materials Research Express

PAPER

Acid hydrogel matrixes as reducing/stabilizing agent for the in-situ synthesis of Ag-nanocomposites by UV irradiation: pH effect

Martin F Broglia[1,2], **Ivana Balmaceda**[1], **Florencia Carrizo**[1], **Cesar A Barbero**[1] **and Claudia R Rivarola**[1]

[1] Institute of Research in Energy Technologies and Advanced Materials (IITEMA), National University of Río Cuarto (UNRC)-National Council of Scientific and Technical Research (CONICET). Chemistry Department, Faculty of Exact, Physical-Chemical and Natural Sciences. National University of Rio Cuarto, Rio Cuarto (Córdoba), Argentina

[2] Engineering Faculty, National University of Rio Cuarto, Rio Cuarto (Córdoba), Argentina

E-mail: crivarola@exa.unrc.edu.ar

RECEIVED
3 December 2018

REVISED
19 December 2018

ACCEPTED FOR PUBLICATION
7 January 2019

PUBLISHED
8 February 2019

Keywords: photoreduction, Ag-nanoparticles, acidic hydrogels, antibacterial nanocomposite

Abstract

Synthetic methods to obtain Ag-nanocomposites are widely studied in order to produce antimicrobial materials without using harmful agents for possible applications in biologic systems. In this way, the nanocomposites could be able to apply in biomedicine area avoiding going through exhaustive processes of purification. Biocompatible hydrogel based on N-isopropylacrylamide (NIPAM) copolymerized with different proportions of methacrylic acid (MAA) and 2-acrylamido-2-methylpropanesulfonic acid (AMPS), were proposed as matrixes of Ag-nanocomposites. A comprehensive study of the physicochemical behavior, reducing and stabilizing character of the matrixes were carried out at pH 2 and 7. Hydrogel nanopores were used as photoreducing of Ag^+ ions and stabilizing of Ag nanoparticles (Ag-NPs) at the same time. Most of the matrixes showed high reducing character at pH 7 while at pH 2 it was significantly reduced. Photoreducer character at pH 7 increased with MAA co-monomer concentration and Ag-NPs sizes of 4–5 nm were obtained. In addition, it was demonstrated that acidic co-monomers favor the stabilization of Ag-NPs avoiding agglomerations. It was possible to conclude that the photoreduction reaction takes mainly place at pH 7 when non bonding electron pairs from carboxylic and amide groups of the matrix are available. Therefore, biocompatible and antimicrobial nanocomposites can be easily synthesized without using damaging additives (reducer, solvent) and be applied in biomedicine.

1. Introduction

Hydrogels are crosslinked hydrophilic polymers capable to absorb large amount of water and remain insoluble in aqueous solutions [1]. Due to the remarkable characteristic of hydrogels such as large swelling in water, high aqueous content, elasticity similar to natural tissues, biocompatibility and low toxicity, they have been used as polymeric matrix in the field of drug delivery [2], immobilization of enzymes [3], formation of nanocomposites with metallic nanoparticles [4], absorbent pads and numerous biomedical applications [5, 6]. Depending on the nature of the polymeric network, they could show changes in its dynamic properties varying the external conditions such as pH, temperature, ionic strength [7–11]. In addition, it is possible to improve the properties of hydrogels and include multiple functionalities by the incorporation of different entities into hydrogels through physical blending or interpenetrating network structure (IPN) or polymeric composite formation [12–14].

It is known that crosslinked hydrogels synthesized at room temperature by radical free polymerization contain internal nanopores able to absorb nanoparticles or act as nanoreactors [15, 16]. The incorporation of metallic or polymeric nanoparticles into polymeric matrices has been proved to be an effective method to enhance the functionality of the polymeric nanomaterials such as thermal, electrical, mechanical, optical properties, etc. In this way, nanocomposites can be widely used as optics materials, electricity materials, biomedical materials, informatics materials, sensor/actuator materials and other [17–20].

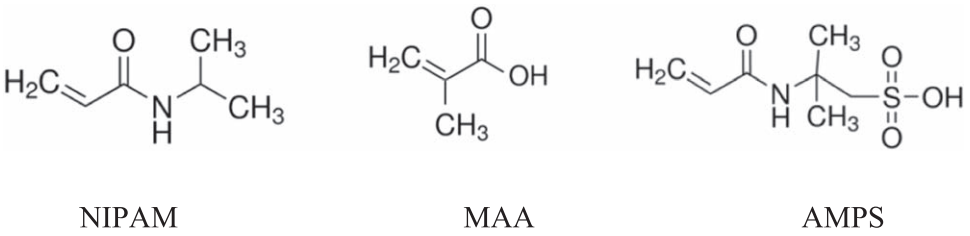

Figure 1. Chemical structure of monomers.

Our interest in manufacturing of polymeric nanocomposites containing silver nanoparticles (Ag-NPs) is mainly due to the excellent antimicrobial effects [21, 22] of those materials while electrical conductivity [23], and optical properties [24] could also be exploited for other applications.

A technique commonly used to incorporate nanoparticles inside hydrogels involves *in situ* chemical reduction of precursor metal ions. However, this usually requires using reducing agents and/or harmful solvents to environmental and biological systems, such as sodium borohydride, hydrazine, and dimethylformamide [25]. Previously, the synthesis of Ag-NPs inside hydrogel by *in situ* photoreduction of Ag^+ ions was proposed as a new alternative to avoid the use of strong reducing agents not compatible with biomedical applications [26]. It was shown that hydrogels made of crosslinked acrylamides are able to photoreducing Ag^+ ions by absorption of UV irradiation avoiding the presence of toxic chemical reactive and generating antibacterial nanocomposites. In that case, the amide groups were proposed as the possible photoreducing agents.

In this work, acidic hydrogels obtained by copolymerization of *N*-isopropylacrylamide (NIPAM) and methacrylic acid (MAA) monomers were proposed as matrixes generator of Ag-nanocomposites. Biocompatibility of matrixes based on NIPAM [27, 28] and the antibacterial effect of Ag-nanocomposites based on these matrixes were previously demonstrated [26].

The ionization state effect about the swelling, adsorption and photoreducer capacity of Ag^+ ions was studied at pH different. NIPAM was also copolymerized with 2-acrylamido-2-methylpropanesulfonic acid (AMPS) to compare the different acid group behavior. This synthetic method allowed obtaining Ag-NPs of 4–5 nm which begin to agglomerate with increasing irradiation time. An analysis of Ag-NPs size distribution allowed discussing about stabilizer character of matrixes. Biocompatible matrixes based on NIPAM and acid co-monomers can be used as reducting/stabilizing agents of Ag-NPs allowed easily obtaining antimicrobial nanocomposites free of toxic agents.

2. Materials and experimental methods

2.1. Reactive

Hydrogel matrixes were synthesized via free radical polymerization of N-isopropylacrylamide (NIPAM) (Scientific Polymer Products, Inc. (USA)) copolymerized with 2-acrylamido-2-methylpropanesulfonic acid (AMPS) (Scientific Polymer Products, Inc. (USA)) or methacrylic acid (MAA). N, N-methylenebisacrylamide (BIS) (Sigma-Aldrich, Argentina) was used as crosslinker agent. Ammonium persulfate (APS) (Sigma-Aldrich, Argentina) and N, N, N′, N′-tetramethylenediamine (TEMED) (Sigma-Aldrich, Argentina) were used as the initiator and activator of polymerization, respectively. The chemical structures of the monomers are shown in figure 1.

2.2. Synthesis of hydrogels

PNIPAM-co-x%MAA copolymers were synthesized by free radical polymerization. NIPAM (0.5 M) and the corresponding percentage (x%) of methacrylic acid (MAA) were dissolved in distilled water to obtain copolymeric hydrogels with 1%, 2% and 5% of MAA (mol percentage based on NIPAM moles). PNIPAM-co-2% AMPS copolymer was also synthesized to compare the effect of different acids. In all cases, 2% BIS (mol based on NIPAM moles) was used as crosslinker agent. Ammonium persulfate (0.003 g ml^{-1}, APS) and N, N, N′, N′-tetramethylethylenediamine (30 μl ml^{-1}, TEMED) were used as redox initiator and activator, respectively. Dissolved O_2 was purged by bubbling with N_2 gas. Polymerization reactions were carried out for 3 h at room temperature.

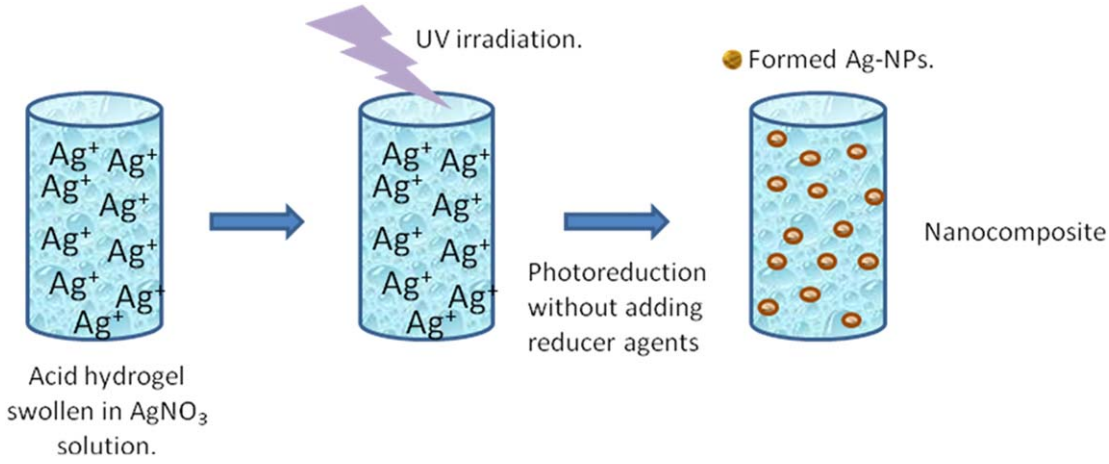

Figure 2. Experimental design of nanocomposite formation by *in situ* photoreduction of Ag^+ ions.

2.3. Synthesis of nanocomposites by in situ photoreduction of Ag^+ ions

Dry hydrogel pills (~0.010 grams each one) were submerged in 3 ml of $AgNO_3$ solution at 0.01 M during 24 h to ensure that maximum swelling was reached. Swollen pills have a size around 1.0 ± 0.1 cm of diameter and 0.20 ± 0.05 cm of thickness. Then, UV light was irradiated on the swollen hydrogels loaded with Ag^+ ions during different time lapses in order to find the time required to obtain the highest concentration of Ag-NPs inside hydrogel (figure 2). The used fluorescent UV lamp (E27 black, Alic SA, Argentina) has the following characteristics: emission wavelength = 365 nm, power = 20 W, frequency = 50 Hz. Ag-NPs formation inside the hydrogels were corroborated by UV-visible spectroscopy and Transmission Electron Microscopy.

2.4. Quantification of Ag-NPs formed inside matrixes by UV-visible spectroscopy

The optical properties of Ag-NPs inside hydrogels were studied by UV–visible spectroscopy (Hewlett-Packard-8453 diode array, Palo Alto, California, USA). To verify the formation of Ag-NPs inside hydrogel, nanocomposite was located between two quartz slides with a separator of 4 mm and was positioned in the spectrophotometer so that the UV-visible light source passes through composite, allowing to obtain the absorption spectra (figure 3). Ag-NPs formation kinetic was followed at 420 nm as a function of irradiation time. Obtained results averaged out at five measurements.

2.5. Swelling capacity of hydrogel matrixes

The swelling capacity of the synthesized hydrogels as a function of irradiation time was studied through gravimetric analysis. The dry hydrogels were weighed (M_s) and then placed it in glass beakers with solutions at pH 2 and 7, adjusted with HCl and NaOH respectively. At different times wet gel was weighed (M_h) after remove the excess water (superficial) with tissue paper. The swelling percentage (%Sw) was calculated by application of the following equation:

$$\%Sw = \frac{(M_h - M_s)}{M_s} x100 \quad (1)$$

Graphics of %*Sw* versus time were made to analyze the swelling kinetic of hydrogel matrixes. %*Sw* obtained data were averaged out at five measurements.

2.6. Determination of the partition coefficient (Pc) of Ag^+ ions.

The partition coefficient (*Pc*) was defined as the distribution of solute ($AgNO_3$) between the hydrogel and liquid phase (water) in equilibrium state. That is, the grams of Ag^+ ions (solute) loaded per 1000 g of hydrogel (molal) rationed to the grams of Ag^+ ions per 1000 g of aqueous solution (molal) after reaching the equilibrium state. Knowing the initial (before swelling) and final moles of Ag^+ ions (after swelling) in the external solution, the concentration of $AgNO_3$ into hydrogel and water, respectively, can be calculated and then *Pc* can be estimated according equation (2):

$$Pc = \frac{moles_{Ag^+}/1000g_{Hydrogel}}{moles_{Ag^+}/1000g_{Solvent}} \quad (2)$$

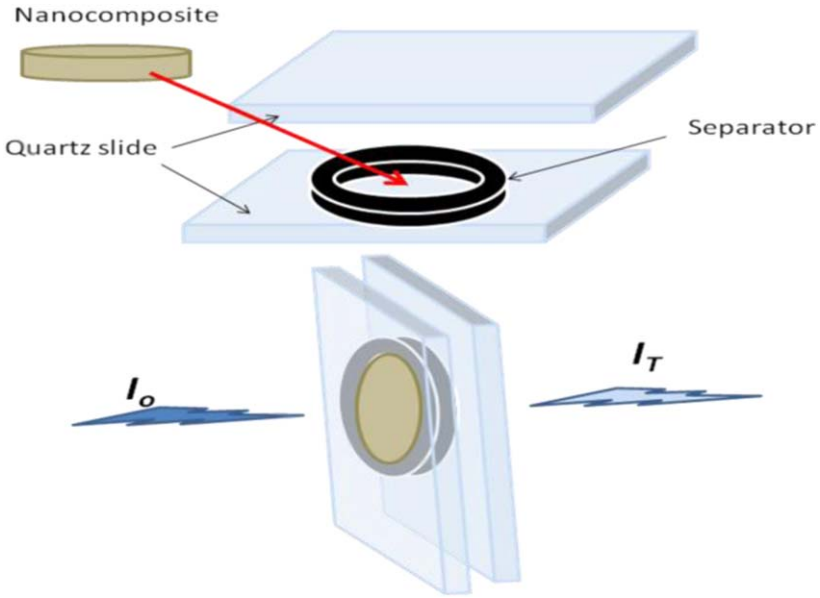

Figure 3. Device to obtain the absorption spectra of nanocomposites by UV-visible spectroscopy.

Experimentally, a piece of dry hydrogel (around 0.010 g) of known mass was immersed in 5 ml of 0.01 M $AgNO_3$ at different pH values (pH 2 and 7). After 24 h of immersion the hydrogel was removed and the concentration of Ag^+ ions remaining in the solution was determined by potentiometric titration with NaCl solution (0.01 M). The swelling procedures were carried out in triplicate. Potentiometric titration was performed employing an ion-selective electrode Ag/AgCl (Methrom AG, Suiza) and a saturated calomel electrode as reference electrode.

2.7. Differential scanning calorimetry (DSC)

The volume phase transition temperature (VPTT) of hydrogel matrixes was determined with a TA Instruments 2010 calorimeter (New Castle, USA) with nitrogen flow. Sample of wet gel (5 mg) was placed and sealed in a cell of aluminum. Then, it was placed inside the chamber of the DSC and cooled to –20 °C surrounding the aluminum chamber with a cooling solution (80% p/p $CaCl_2$ solution). It was left 5 min until the temperature reached equilibrium state. Then the system was heated at a rate of 10 °C min^{-1} from −20 °C to 60 °C.

2.8. FTIR- spectroscopy

The Fourier transform infrared spectroscopy (FITR) spectra of dry hydrogel matrixes were performed in a Bruker Tensor 27 FTIR spectrometer (Madison, Wis. USA) with a resolution of 4 cm^{-1}. The polymer sample was mixed with finely milled KBr (Aldrich) and the pellets were obtained by pressing powder for 15 min at 15 Tn cm^{-2} under dynamic vacuum.

2.9. Transmission electronic microscopy (TEM)

Transmission electronic micrographs of nanocomposites were taken in a Jeol Jem-1220 (Jeol USA, Inc.) transmission electron microscope. The images of formed Ag-NPs size during irradiation times were analyzed by Image J program and the diameter distribution histograms were fitted by a Non-Lineal Curve Fit (Log-Normal function). Thence two parameters were considered according to equation (3): diameter (D_0) and standard deviation (σ), and the maximum diameter (D_{max}) of distribution can be calculated.

$$D_{max:} = Do \exp(-\sigma^2) \quad (3)$$

3. Results and discussion

3.1. Chemical characterization of hydrogel matrixes by FTIR

FTIR spectra were taken to identify the main functional groups of copolymers. FTIR of PNIPAM, PNIPAM-co-5%MAA PNIPAM-co-2%AMPS hydrogels were shown in figure 4. Characteristic bands of PNIPAM were observed in all samples, at 1640 cm^{-1} (C=O stretching of amide I), at 1540 cm^{-1} (N– H bending of amide II), at 1177 cm^{-1} (C–N of amide III), and the bands assigned to the isopropyl groups (C–$(CH_3)_2$) at 1387 cm^{-1}. The

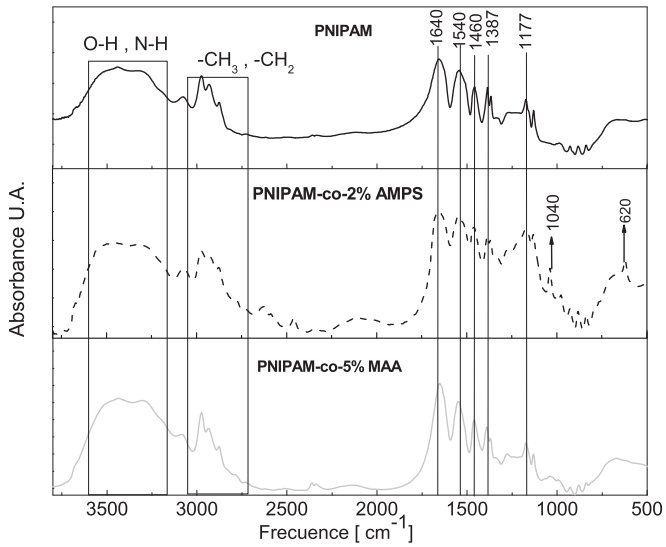

Figure 4. FTIR spectra: PNIPAM, PNIPAM-co-2%AMPS and PNIPAM-co-5%MAA hydrogels.

Table 1. Phase transition temperature (VPTT) of the hydrogel swollen in water at pH 7 and pH 2.

Hydrogels	VPTT[a]/°C	
	pH 2	pH 7
PNIPAM	34.6	32.6 [36]
PNIPAM-co-1%MAA	35.2	33.2
PNIPAM-co-2%MAA	34.7	33.5
PNIPAM-co-5%MAA	36.9	35.9
PNIPAM-co-2%AMPS	38.2	36.8 [37]

[a] Error: ± 0.5 °C.

absorption bands at 1459 cm^{-1} were attributed to C–H bending in (C–$(CH_3)_2$) and –CH_2—groups. The bands at 2924 cm^{-1} and 2849 cm^{-1} were related to the stretching of –CH_3 and –CH_2– groups in the polymeric chain.

A broad peak from 3100 to 3600 cm^{-1} was due to the presence of both N-H and O-H groups [29, 30], where one of them corresponds to N-H stretching (3440 cm^{-1}) of NIPAM monomers and the other to O-H stretching (3300 cm^{-1}) due to co-monomers. In addition, the MAA and AMPS monomers have different functional groups (carboxylic and sulfonic), which can also be identified by FTIR spectroscopy [31]. For the copolymer containing AMPS monomeric units, the characteristic bands of the sulfonic groups such as 1192–1040 cm^{-1} (asymmetric and symmetric O=S=O stretching) and 620 cm^{-1} (st. C–S) were observed [32, 33].

3.2. Volume phase transition temperature (VPTT) of hydrogel matrixes

The volume phase transition temperatures (VPTT) of synthesized hydrogels were obtained by DSC and shown in table 1. The results indicated that only when the matrix contents 5% MAA a significant increasing of VPTT was noted with respect to PNIPAM value. To similar proportions of acidic monomers (2%AMPS or 2%MAA) an increasing of 3–4 °C of VPTT was observed for AMPS independently of solution pH. It is known that sulfonic acids are much stronger acids than the corresponding carboxylic acids. For example, it was reported to MAA, which contain a carboxylic acid functional group, a value of pKa = 4.46 [34] while AMPS, which contain a sulfonic acid (-SO_3H) functional group, is dissociated completely in the overall pH range ($EtSO_3H$, pKa (water) = −1.68) [29, 35]. In addition, amide groups can change its ionized states in function of pH. Therefore, the observed changes in VPTT could be directly related to the different interactions that are present inside the hydrogel matrix depending of medium pH as hydrogen bonding and electrostatic repulsion.

3.3. Swelling behavior of the hydrogel matrixes

One of the major physicochemical characteristics of hydrogels is the capacity to swell or uptake water. When hydrogels contain weak acid groups, it is possible that the swelling depends on medium pH. Therefore, the swelling kinetic of PNIPAM-co-x%MAA hydrogel were studied at pH 2 and 7 (around pKa) to compare the

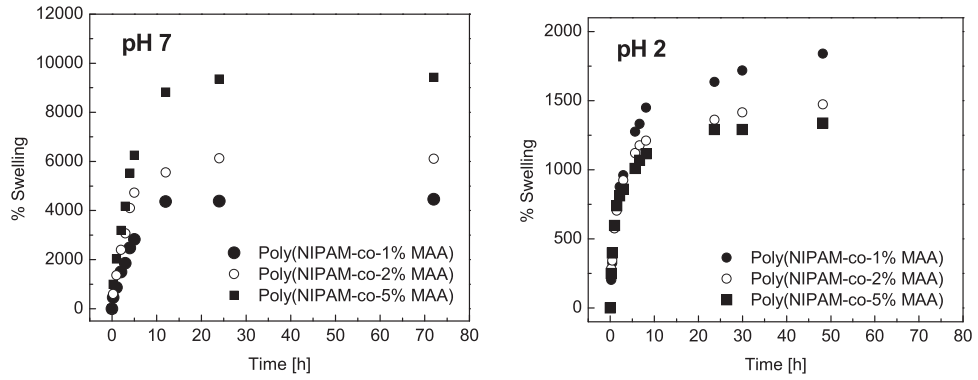

Figure 5. Dynamic swelling behavior of PNIPAM-co-xMAA composed by 1%, 2% and 5% of MAA at pH 7 and pH 2.

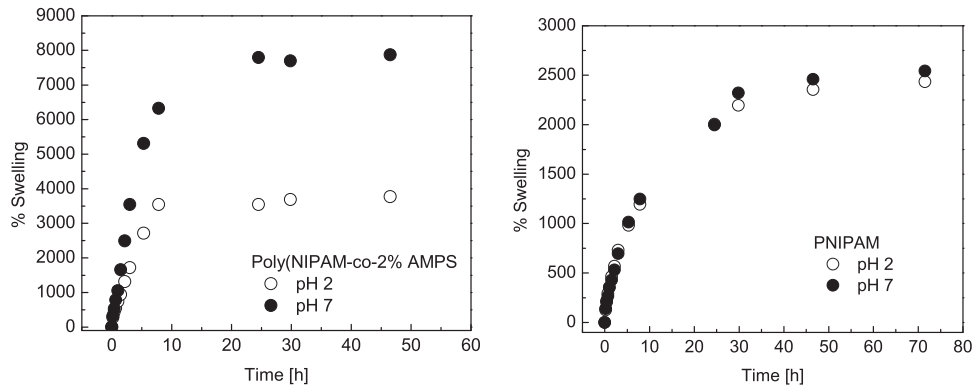

Figure 6. Dynamic swelling behavior of PNIPAM and PNIPAM-co 2%AMPS at pH 7 and pH 2.

behavior of the ionized and no-ionized states of functional groups. At same time, PNIPAM-co-2%AMPS and PNIPAM were also analyzed in similar conditions.

In figure 5, it can be seen that the %Sw increased with time in both pH values until it reaches a plateau. The value of %Sw at the plateau is called swelling capacity maximum of hydrogel in equilibrium state (% Sw(eq)). Noteworthy, higher values of % Sw(eq) were achieved at pH 7 (ca 8 times more than at pH 2) for PNIPAM-co-x%MAA. At pH 7, electrostatic repulsion between $–COO^{-}$ groups are present due to the carboxylate groups. On the other hand, hydrogen bonding (between –COOH groups) is present at pH 2. However, a stronger effect involves the osmotic pressure due to mobile counterions (e.g. Na^{+}) of the –COO- groups, only present at pH 7. Accordingly, the values of % Sw(eq) increased with the content of MAA in the copolymer since increased the relative amount of $–COO^{-}$ groups. At pH 2, the % Sw(eq) decreased when the content of MAA increased because carboxylic (-COOH) groups present stronger interactions (hydrogen bonding) than alkyl amide groups [10].

In figure 6, it can be seen that swelling kinetic of PNIPAM was not altered by pH while for PNIPAM-co- 2% AMPS a pH effect was notable. The same behavior was noted in previous work [35] where %Sw(eq) at pH 10 is larger than at pH 4. It is likely that the ionic force was different at pH 2 and 7 due to the different nature of the main cations (Na^{+} and H^{+}) present at pH 7 and 2.

The table 2 resumes the % Sw(eq) changes (Δ% Sw(eq)) defined as the difference between % Sw(eq) at pH 7 and 2. It can be seen that the swelling kinetic of PNIPAM does not depend of solution pH due to Δ% Sw(eq) was within range of observed errors. Lower swelling capacity of PNIPAM-co-x%MAA than PNIPAM was observed at pH 2 possibly because the presence of intramolecular hydrogen-bonding interactions through carboxylic and amide groups. However, the electrostatic repulsion at pH 7 between carboxylic groups was more important and % Sw(eq) increased with %MAA. PNIPAM-co-2%AMPS presented high % Sw(eq) at both pH but the Δ% Sw(eq) was similar to PNIPAM-co-2%MAA. It is say; the acidic force of co-monomer might not favor the swelling capacity of acid matrix.

3.4. Kinetic parameters of water diffusion in hydrogel matrixes

In order to study more exhaustively the effect of pH and acid composition of hydrogel matrixes, the diffusion mechanisms of water at pH 7 and 2 were analyzed. The kinetic of water diffusion into hydrogel was determined

Table 2. Swelling capacity percentage (%Sw(eq)) in equilibrium states and the changes (Δ%Sw(eq)) observed at both pH.

Hydrogels	% Sw(eq)[a]		Δ% Sw(eq)
	pH 2	pH 7	pH 7—pH 2
PNIPAM	2560	2450	−110
PNIPAM-co-1%MAA	1840	4450	2610
PNIPAM-co-2%MAA	1460	6145	4685
PNIPAM-co-5%MAA	1330	9420	8090
PNIPAM-co-2%AMPS	3730	7860	4130

[a] Error:±100

with the following equation [38, 39]:

$$F = \frac{M_t}{M_\infty} = kt^n \tag{4}$$

where F denotes the amount of solvent fraction at time t, M_t denotes the amount of water diffused inside the matrix at time t (difference between the swollen hydrogel mass at time t and dry hydrogel mass), M_∞ corresponds to the amount of water that has diffused inside the matrix at equilibrium state (difference between the swollen hydrogel mass at equilibrium state and dry hydrogel mass) and k is a constant related to the structure of the network. The exponent 'n' determines the type of diffusion mechanism of water. For samples of cylindrical shape the diffusion is Fickian if n is in the range of 0.45–0.50, whereas the diffusion is non-Fickian type if $0.50 < n < 1.00$. The diffusion mechanism is anomalous or non-Fickian, when both diffusion and polymer relaxation control the overall rate of water uptake [40].

Appling logarithm to equation (4), it is possible determinate the n value from the initial slope of plots of ln *F* as a function of ln *t*, according equation (5).

$$\ln F = \ln k + n \ln t \tag{5}$$

The representative curves of lineal behavior of swelling kinetics of hydrogels according equation (4) were shown in figure 7 at pH 7 and 2. From the fitting of these curves *n* and ln *k* values were determined and reported in the table 3.

The obtained values of *n* were higher than 0.5 for all the studied hydrogels, even when the pH of the external medium increased from 2 to 7. This indicates that the water sorption occurs through a non-Fickian mechanism. This is generally explained as consequence of slow relaxation rate of the polymer matrix (diffusion relaxation controlled process) [41]. The relatively slow relaxation rate of the polymeric matrix is similar to the diffusion rate of the solute (water). Although size of water molecule is small, the slow relaxation rate of matrix does not permit the free intake of it. This means that the chains need relatively large times to adapt themselves for the penetration of water molecules and adopt a new equilibrium conformation [42].

Another parameter that can be obtained through the analysis of swelling kinetic is the diffusion coefficient (D) of solvent for each kind of hydrogel. For that, the method of approximating short time can be applied considering that it is valid until a 60% of the hydrogel swelling in the selected solvent. Taking into account the geometric parameters of matrix, the equation (4) is re-defined as [39]:

$$F = 4\left[\frac{D}{\pi L^2}\right]^{1/2} t^{1/2} \tag{6}$$

where *D* is the diffusion coefficient ($cm^2\ s^{-1}$), *t* is the time (seconds), *L* is the radius of the cylindrical polymer (cm) and *F* is the fraction of diffused solvent inside the polymeric matrix at time *t*.

Graphs of *F* versus $t^{1/2}$ were performed for all the hydrogels (figure 8) and the diffusion coefficients were obtained from the slope of the curves following the equation (7):

$$D = \left(\frac{\pi L^2 (slope)^2}{16}\right) \tag{7}$$

The obtained *D* values (table 3) were according to values previously reported of water diffusion coefficients in 1-propanol ($5.0 \times 10^{-6}\ cm^2\ s^{-1}$) [43] and PNIPAM for non-Fickian diffusion process ($4.5 \times 10^{-7}\ cm^2\ s^{-1}$ at 25 °C) [44]. Also, it was reported for PNIPAM values of $n > 0.5$ and $D = 7.7 \times 10^{-9}\ cm^2\ s^{-1}$ at 20 °C [37]. PNIPAM presents a *D* value higher than the other matrixes possibly due to there are not electrostatic interactions between matrix and water. The obtained *D* values for PNIPAM-co-x%MAA increased with the percentage of MAA monomer. However, it seems that these were not very affected by pH changes. The k values are not always reported but it can be seen that they had the same tendency that *D* values.

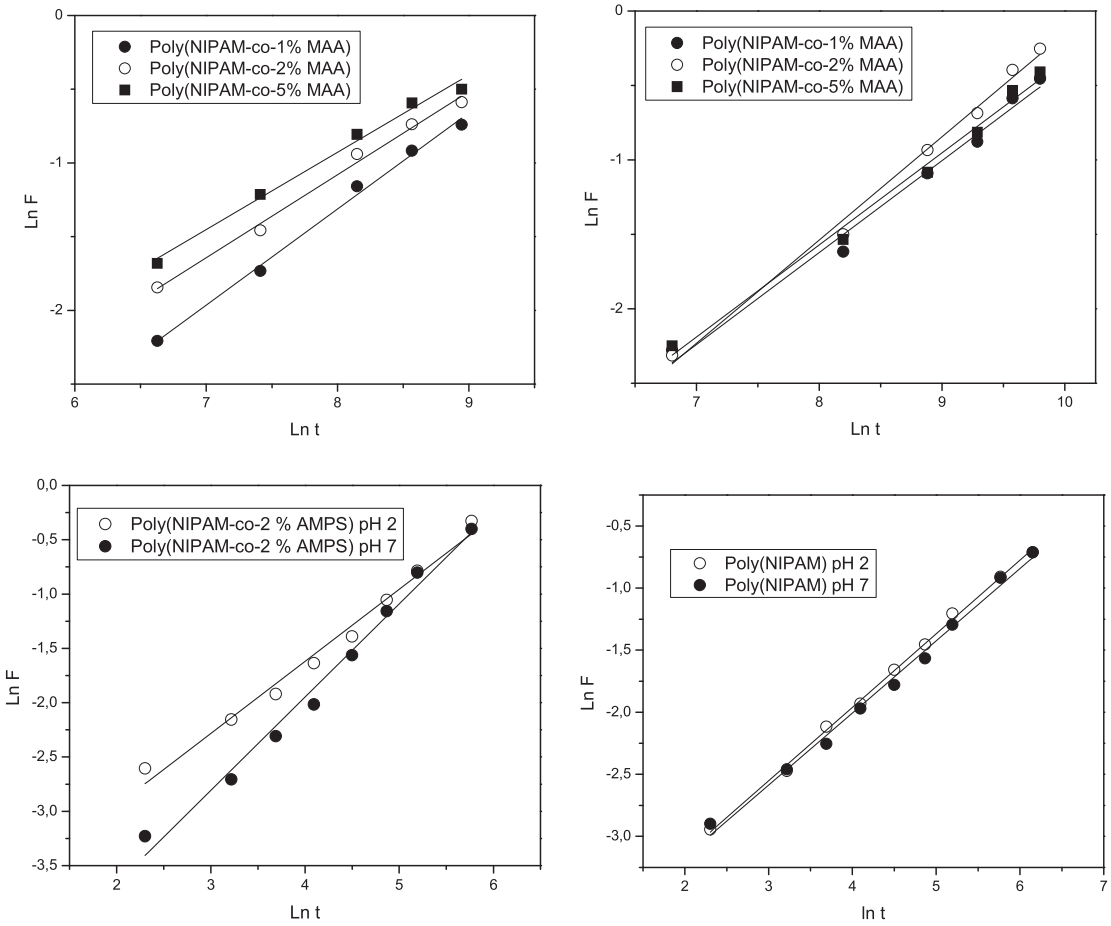

Figure 7. Swelling kinetics curves of hydrogels at pH 2 and pH 7 analyzed by equation (4).

Table 3. Effect of acid monomer content and medium pH on the swelling kinetic parameters of hydrogels according Ec (4) and diffusion coefficients of water according Ec. (6–7) determined at 25 °C.

pH 2	n	k	D $cm^{-2}s^{-1}$
PNIPAM	0.58	1.3×10^{-2}	3.71×10^{-5}
PNIPAM-co-1%MAA	0.65	1.45×10^{-3}	1.86×10^{-6}
PNIPAM-co-2%MAA	0.56	4.08×10^{-3}	2.43×10^{-6}
PNIPAM-co-5%MAA	0.52	6.03×10^{-3}	3.07×10^{-6}
PNIPAM-co-2%AMPS	0.69	1.4×10^{-3}	1.46×10^{-6}
(radium hydrogels: 1% MAA, 2% MAA, 5% MAA 0.5 cm and 2% AMPS 0.6 cm)			
pH 7	n	k	D $cm^{-2}s^{-1}$
PNIPAM	0.59	1.3×10^{-2}	4.01×10^{-5}
PNIPAM-co-1%MAA	0.62	1.41×10^{-3}	1.32×10^{-6}
PNIPAM-co-2%MAA	0.69	8.33×10^{-4}	2.58×10^{-6}
PNIPAM-co-5%MAA	0.61	1.48×10^{-3}	2.80×10^{-6}
PNIPAM-co-2%AMPS	0.85	4.6×10^{-3}	2.50×10^{-6}

(Radium hydrogels: 0.5 cm (1% MAA), 0.55 cm (2% MAA), 0.7 cm (5% MAA) and 0.8 cm (2%AMPS))

Considering that the diffusion coefficients of water depend on chemical composition of matrixes and the swelling capacity depend on solution pH, a study about the capacity of the hydrogels to adsorb Ag^{+} ions at both pH is also necessary.

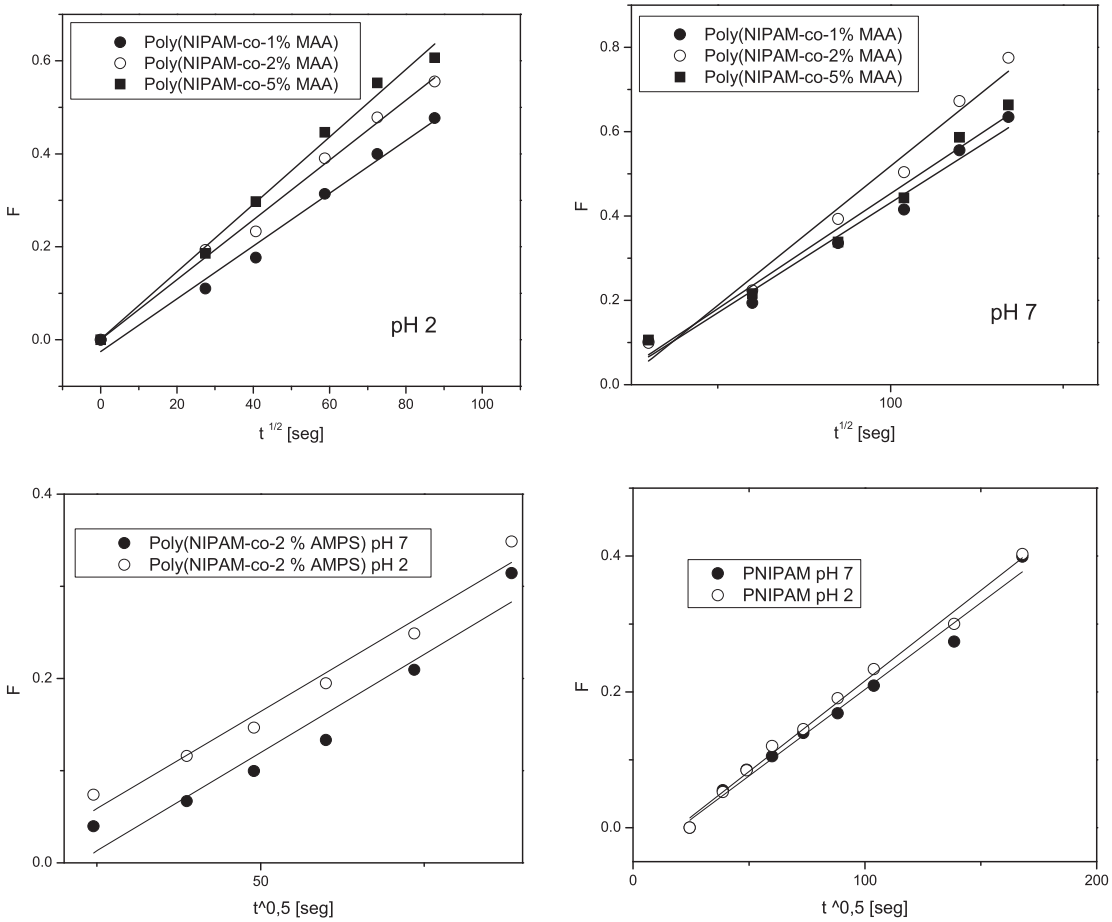

Figure 8. Swelling kinetic curves of F versus $t^{1/2}$ for hydrogels at pH 2 and pH 7 (equation (6)).

Table 4. Partition coefficients (Pc) of Ag^+ ions determined in hydrogel/water at 25 °C at pH 2 and pH 7.

Hydrogels	Pc (pH 2)	Pc (pH 7)
PNIPAM	29.1 ± 5, 5	42.2 ± 2.9
PNIPAM-co-1%MAA	15.5 ± 0.9	32.6 ± 2.6
PNIPAM-co-2%MAA	16.6 ± 3.6	42.0 ± 1.0
PNIPAM-co-5%MAA	17.5 ± 2.0	53.9 ± 2.1
PNIPAM-co-2%AMPS	20.1 ± 1.5	28.9 ± 0.4

3.5. Partition coefficients of Ag^+ ions

To know the capacity of the matrix to absorb Ag^+ ions, it is required to determine the partition coefficient of ions between hydrogel and water. Partition coefficients (Pc) of $AgNO_3$ were calculated according to equation (2). Values of Pc $>$ 1 indicate that Ag^+ ions were incorporated mainly into hydrogel. In this case, the hydrogel could be used as a possible photoreducer matrix of ions. The Pc values calculated from hydrogels loaded with 0.01 M of $AgNO_3$ at 25 °C were shown in table 4.

Experimental results indicated that Pc values were dependent on medium pH. Previously, it was also demonstrated that the swelling capacity and VPTT of PNIPAM matrix were slightly affected by pH changes. Noteworthy, PNIPAM has more capacity to take Ag^+ ions (high Pc values) than other hydrogels at pH 2. This can be due to the fact that acid matrixes are in protonated state (without ionic charges) so have lower swelling capacity than PNIPAM which avoiding the entering of ions.

In all cases, the Pc values at pH 7 were mayor than at pH 2, being notable that the partition of Ag^+ ions between hydrogel/water was favored with %MAA.

PNIPAM-co-2%AMPS was an exceptional case with a behavior similar to previously reported work [26]. Possibly, lower Pc value at pH 2 than pH 7 is related to the low swelling capacity of matrix at that pH or with the absence of anionic groups to interact with Ag^+ ions.

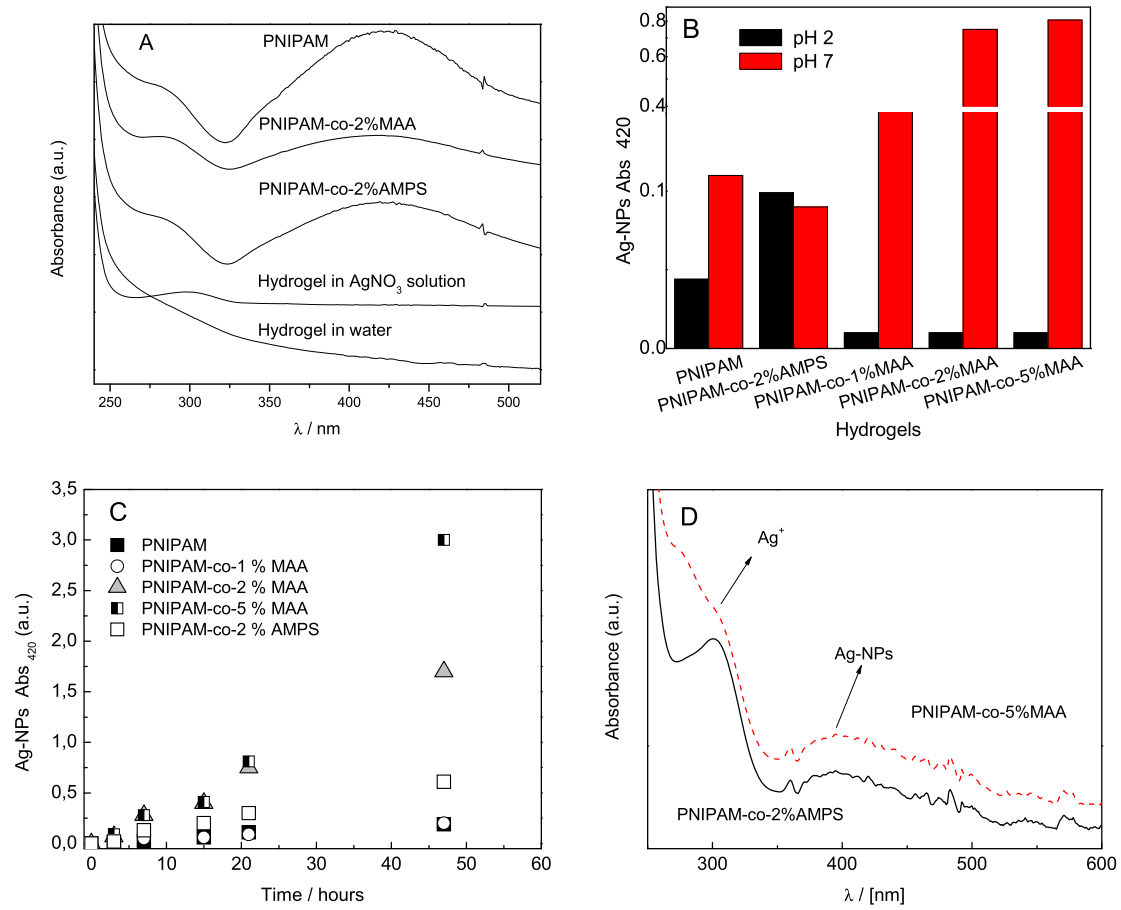

Figure 9. (A) UV visible spectra of *in situ* formed Ag-NPs in different hydrogel matrixes by application of UV light during 15 h at pH 7 and UV visible spectra hydrogel swelling in water and in $AgNO_3$ solution at 0.01 M before irradiation. (B) Absorbance at 420 nm of formed Ag-NPs by irradiation during 22 h at pH 2 and pH 7 in each matrix. (C) Kinetic of Ag-NPs formation by UV irradiation following at 420 nm and pH 7. (D) UV spectra of Ag^+ ions and Ag-NPs in aqueous solution released from nanocomposite after 72 h.

3.6. Synthesis of AgNPs-hydrogel nanocomposites by UV radiation: pH effect

In order to analyze the effect of acid groups present in the matrix on the formation kinetic of Ag-NPs, the *in situ* photoreaction was carried out at pH 2 and 7 as a function of time. The Ag-NPs formation was analyzed by UV-visible spectroscopy and TEM.

Absorption spectra of nanocomposites obtained by UV irradiation after 15 h at pH 7 were shown in figure 9(A). The absorption band at 290 nm corresponds to Ag^+ ions and matrix [45] and the band with maximum at 420 nm corresponds to formed Ag-NPs absorption. Figure 9(B) shows the absorbance of Ag-NPs at 420 nm after 22 h of irradiation for both pH values. At the same irradiation time, the photoreduction of Ag^+ ions seems to be inhibited at pH 2. At pH 7 the amount of formed Ag-NPs significantly increased with %MMA at same time of irradiation.

The Ag-NPs formation kinetic shown in figure 9(C), confirms that higher percentage of MMA favor the amount of formed Ag-NPs at same irradiation time and pH 7, since that the absorbance of Ag-NPs of PNIPAM-co-2%MAA and PNIPAM-co-5%MAA were greater than the obtained in the matrix others at the same irradiation time. It could be indicated that the non bonding electron pair of carboxylate groups of MAA at pH 7 are taking part in the reduction reaction of Ag^+ ions. Therefore, the photoreducing capacity of matrixes which increasing with MAA co-monomer percentage at pH 7 would be directly related to the higher swelling capacity and partition coefficients of Ag^+ ions.

Most of the researches on Ag^+ ion reduction without addition of a reducting agent do not discuss in detail the reaction mechanism. However, several researchers propose first the coordination between electron pair of nitrogen atom with Ag (catalyzed by AMPS). Then, the electron transfer from nitrogen atoms to Ag(0) happens and a nitrogen radical cation is formed. The radical cation abstract an electron from the water molecule forming a hydronium ion and hydroxyl radical which follows the known secondary reactions [4, 46].

The electron transfer is favored by light absorption and pH $>$ 7 when the n or π electrons are free.

The releasing of antimicrobial species in aqueous solution from the nanocomposite pill was followed by UV spectroscopy. Figure 9(D) show the both of absorption bands of Ag^+ ions at 290 nm and Ag-NPs around 400 nm

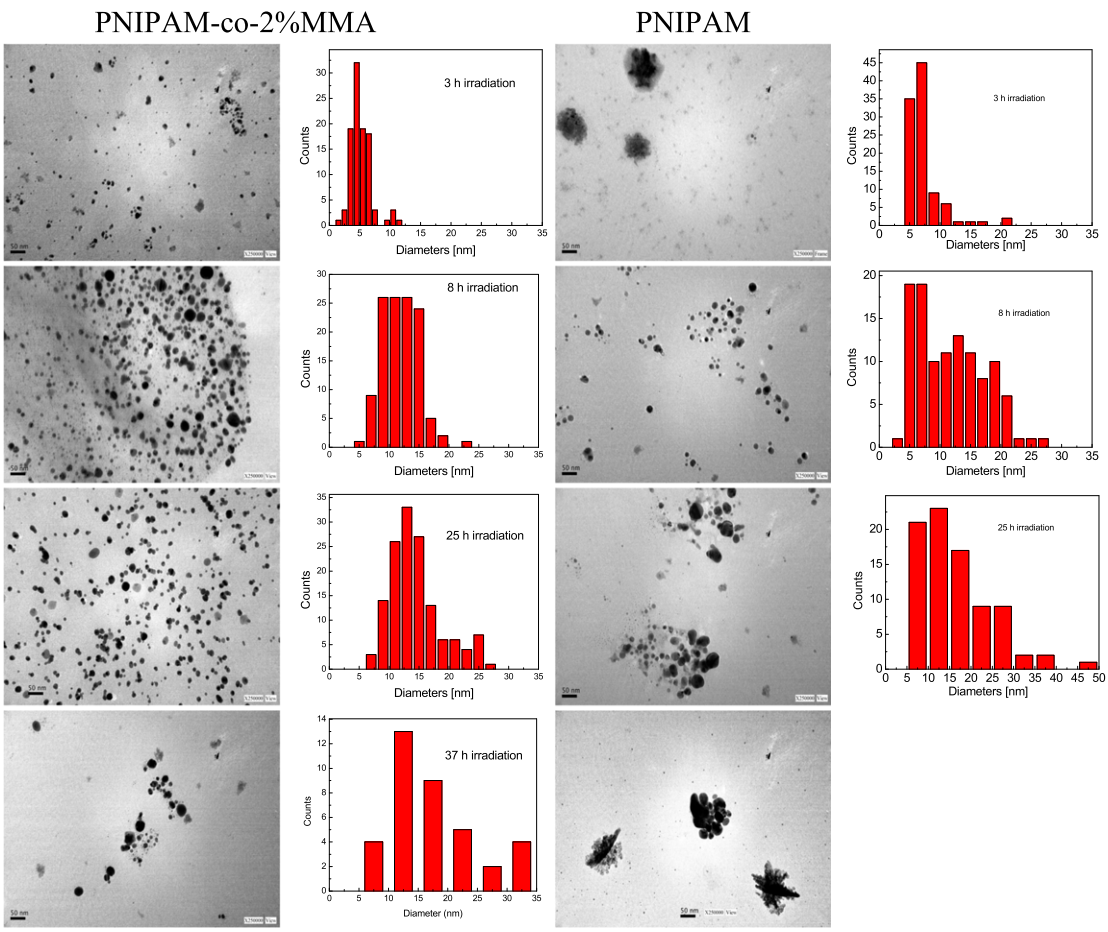

Figure 10. TEM images and the corresponding size distribution analyses of Ag-NPs obtained at different irradiation time of PNIPAM-2%MAA and PNIPAM at pH 7.

Table 5. Ag-NPs maximum diameters obtained from histograms (figure 10).

Irradiation time	Diameter maximum (nm)			
	PNIPAM		PNIPAM-2%MAA	
3 h	4.8 (Narrow)		4.1(Narrow)	10.5 (Low counts)
8 h	5.9 (Low counts)	13.4 (Narrow)	9.6 (width)	
25 h	12.5 (Narrow)	27.0 (Low counts)	11.8 (width)	25.0 (Low counts)
37 h	Spikes were formed		12.2 (width)	34.0 (Low counts)

released in aqueous solution after 72 h of exposition. The releasing of these species explains the antibacterial activity of the nanocomposite.

3.7. Analysis of size and morphology of obtained Ag-NPs at pH 7.

The stabilizing effect of matrixes on Ag-NPs during irradiation was analyzed trough TEM images and the building of size distribution histograms. First, PNIPAM and PNIPAM-co-2%MAA were compared as stabilizer matrixes in function of irradiation time. Size distribution of Ag-NPs in PNIPAM-co-2%AMPS nanocomposite was also measured to analyze the effect of acid character of matrix on NPs formation.

Diameter distribution histograms were obtained from TEM images of Ag-NPs/PNIPAM-co-2%MAA at different irradiation time and shown in figure 10. The analysis of histograms was resumed in table 5. It can be seen that two NPs size distribution peaks or one width distribution peak appear when the irradiation time increases.

At 3 h of irradiation, spherical Ag-NPs with diameters around 4 nm were observed in both matrices but sizes of 10 nm and 20 nm also appeared in PNIPAM-co-2%MAA and PNIPAM respectively.

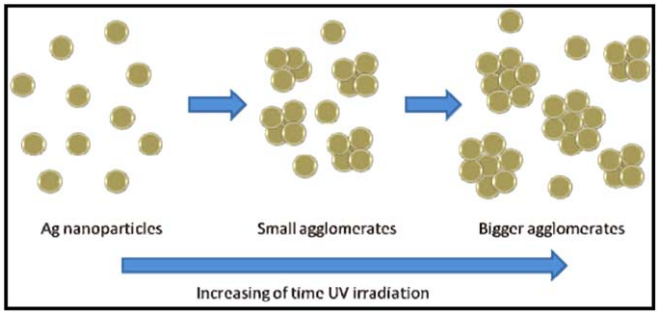

Figure 11. Aggregation process of Ag-NPs formed inside hydrogel matrix.

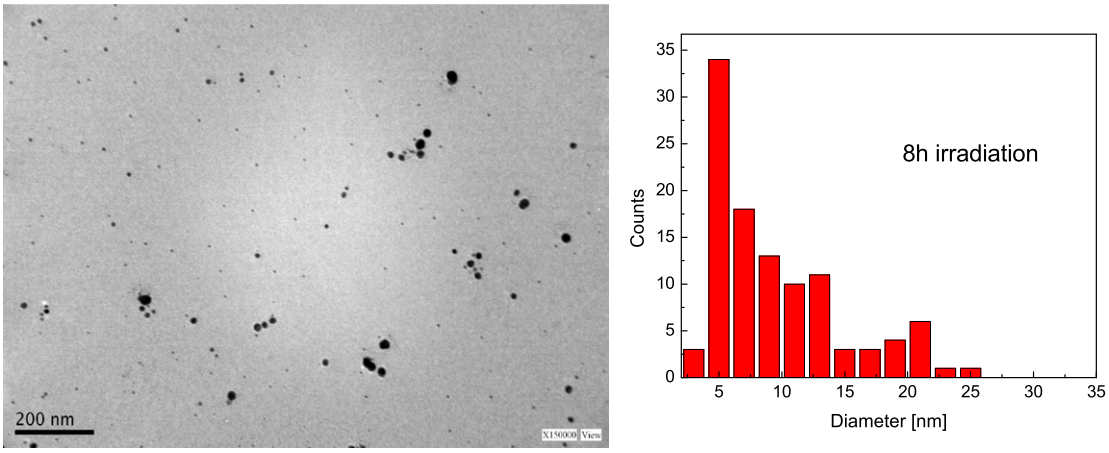

Figure 12. TEM image and histogram of Ag-NPs in the PNIPAM-co-2%AMPS matrix obtained at 8 h irradiation.

At 8 h of irradiation, PNIPAM-2%MAA shown a width size distribution with maximum diameters around 10 nm, while PNIPAM shown two maximum at 5.9 and 13.4 nm until achieving sizes of 20 nm.

When the UV irradiation was applied for 37 h, diameters around 34 nm were obtained in PNIPAM-co-2% MAA nanocomposite, while spike-like particles begin to form in PNIPAM matrix.

In all cases, Ag-NPs with diameters around 6 nm were always present during all irradiation times but an aggregation process are occurring, as it was described in figure 11. When the Ag-NPs concentration increases, they are located in bulk water of pores and in this conditions the Ag-NPs tend to agglomerate due to the Van der Waals forces between colloidal particles [47].

We should remember that the wall pores of the hydrogel are not rigid; the polymeric chains can extend into the aqueous pool inside the hydrogel and increase the volume and the swelling capacity. This allows the agglomerate formation inside bulk pores. Evidence about nanometric domains formed in matrix of hydrogel by semi-interpenetration of PANI (polyaniline) shown sizes in range of 18–280 nm being that the pore size of hydrogel matrix calculated from Flory–Rehner theory was of approx. 45 nm [17].

Apparently, a neutral matrix like PNIPAM is not good stabilizer of NPs since that the Ag-NPs tend to agglomerate more easily inside it. In case of Ag-NPs/PNIPAM-2%AMPS nanocomposite, a narrow distribution of small particle (figure 12) around 5.3 nm and very little amount of big particles were observed at 8 h of irradiation. Analyzing these results with the PNIPAM and PNIPAM-co-2%MAA matrixes at same irradiation conditions, it could be concluded that PNIPAM-2%AMPS matrix has more stabilizing character of Ag-NPs being that smaller Ag-NPs were obtained. So, the anionic character of matrix at pH 7 could be favoring the stabilization of nanoparticles avoiding the agglomerate formation.

Comparing the behavior of PNIPAM, PNIPAM-2%AMPS and PNIPAM-2%MAA matrixes, the difference among them is the presence and force of acid groups. It is evident that acid groups in the polymer backbone help to stabilize the Ag-NPs avoiding agglomerates.

To compare the acid force between -COOH and -SO_3H groups, we must take into account the resonance stabilization (delocalization of π-bond electrons and hence a reduction in energy) of the two molecules. It is

knows that the electron delocalization is greater (spread over more atoms) in the SO_3^- ion than in the—COO^- ion, making –SO_3H a stronger acid than -COOH [25].

At same time, PNIPAM-2%AMPS matrix has more swelling capacity than PNIPAM-2%MAA likely due to a larger activity of the mobile counterions (e.g. Na^+). This is likely related to the weaker interaction of cations with $–SO_3^-$ than with $–COO^-$. In the same sense, sulfonate ions interact more weakly with Ag nanoparticles than carboxylate [48, 49].

The higher swelling capacity implies a increasing of pore size and therefore the superficial area in contact with the NPs would be also increasing. Therefore, both considerations support the observed stronger ability of PNIPAM-2%AMPS matrix walls to stabilize Ag-NPs by surface adsorption.

4. Conclusions

Hydrogels of PNIPAM, PNIPAM-*co*-x%MAA and PNIPAM-*co*–2%AMPS were synthesized through the free radical copolymerization in aqueous solution and room temperature in order to obtain matrixes with molecular porosity or nanoporous. The MAA and AMPS co-monomers in the PNIPAM matrix have an important influence on the kinetics and swelling parameters in water which were significantly affected by the external pH showing a higher degree of swelling at pH 7. In all cases, the swelling exponent *n*, was higher than 0.5 indicating a non-Fickian diffusion process. Diffusion coefficients values of water were similar to previously reported data and it was shown that increased with the MMA content.

All studied hydrogels were able to photoreduce Ag^+ ions in absence of reducing agents and stabilizers. Hydrogels based on PNIPAM and MAA co-polymers presented higher Pc values of Ag^+ ions and stronger photoreducing character at pH 7, while both parameters were significantly reduced at pH 2. Therefore, the higher Ag^+ adsorption capacity inside acid matrix and photoreduction reaction take place when non bonding electron pairs of carboxylic groups coming from MAA are available.

Ag-NPs from 4–6 nm were obtained during irradiation which beginning to agglomerate and form big particles with increasing of irradiation time. Therefore, matrixes with acid co-monomers seem have more capacity to stabilize the Ag-NPs avoiding the agglomeration and possibly this effect would be dependent of acid force.

Antimicrobial nanocomposites can easily be fabricated inside biocompatible hydrogels by UV irradiation without using harmful additive for the environment or biological systems, regulating the proportion and stability of obtained Ag-NPs according to acid matrix composition and time irradiation. Through this proposed synthetic method, the obtained nanocomposites could be able to apply in biomedicine area avoiding going through exhaustive processes of purification.

Acknowledgments

This work was funded by CONICET, FONCYT, and SeCyT-UNRC. I Balmaceda thanks SeCyT-UNRC for a research fellowship. F Carrizo thanks EVC-CIN for a research fellowship. M Broglia, C Barbero and C Rivarola are permanent researcher of CONICET.

ORCID iDs

Claudia R Rivarola https://orcid.org/0000-0002-3944-0949

References

[1] Pó R 1994 Water-absorbent polymers: a patent survey *Polymer Reviews* **34** 607–62
[2] Tonnesen H H and Karlsen J 2002 Alginate in drug delivery systems *Drug Development and Industrial Pharmacy* **28** 621–30
[3] Liu Q, Rauth A M and Wu X Y 2007 Immobilization and bioactivity of glucose oxidase in hydrogel microspheres formulated by an emulsification-internal gelation-adsorption-polyelectrolyte coating method *International. Journal of Pharmaceutics* **339** 148–56
[4] Guocai X, Shengtao G, Xiaoli J and Xiaomei Z 2014 Characterization and synthesis mechanism of nanosilver/PAMPS composites by microwave *Soft Nanoscience Letters* **4** 15–23
[5] Zhao F, Yao D, Guo R, Deng L, Dong A and Zhang J 2015 Composites of polymer hydrogels and nanoparticulate systems for biomedical and pharmaceutical applications *Nanomaterials (Basel)* **5** 2054–130
[6] Caló E and Khutoryanskiy V V 2015 Biomedical applications of hydrogels: A review of patents and commercial products *Eur. Polym. J.* **65** 252–67
[7] Ju H K, Kim S Y, Kim S J and Lee Y M 2001 pH/temperature-responsive semi-IPN hydrogels composed of alginate and poly(N-isopropylacrylamide) *Journal Applied Polymer Science* **83** 1128–39
[8] Gupta P, Vermani K and Garg S 2002 Hydrogels: from controlled release to pH-responsive drug delivery *Drug Discovery Today* **7** 569–79

[9] George M and Abraham T E 2007 pH sensitive alginate-guar gum hydrogel for the controlled delivery of protein drugs *International Journal Pharmaceutics* **335** 123–9
[10] Thakur A, Wanchoo R K and Singh P 2011 Structural parameters and swelling behavior of pH sensitive poly(acrylamide-co-acrylic acid) hydrogels *Chemical and Biochemical Engineering Quarterly* **25** 181–94
[11] Heras Alarcón C, Pennadam S and Alexander C 2005 Stimuli responsive polymers for biomedical applications *Chem. Soc. Rev.* **34** 276–85
[12] Thomas V, Namdeo M, Mohan Y M, Bajpai S K and Bajpai M 2008 Review on polymer, hydrogel and microgel metal nanocomposites: A facile nanotechnological approach *Journal of Macromolecular Science, Part A. Pure and Applied Chemistry* **45** 107–19
[13] Hu Z and Chen G 2014 Novel nanocomposite hydrogels consisting of layered double hydroxide with ultrahigh tensibility and hierarchical porous structure at low inorganic content *Adv. Mater.* **26** 5950–6
[14] Merino S, Martin C, Kostarelos K, Prato M and Vazquez E 2015 Nanocomposite hydrogels: 3D polymer-nanoparticle synergies for on-demand drug delivery *ACS Nano* **9** 4686–97
[15] El-Sherif H, El-Masry M and Kansoh A 2011 Hydrogels as template nanoreactors for silver nanoparticles formation and their antimicrobial activities *Macromolecular Research* **19** 1157–65
[16] Soto-Quintero A, Romo-UribeÁ., Bermúdez-Morales V H, Quijada-Garrido I and Guarrotxena N 2017 3D-hydrogel based polymeric nanoreactors for silver nano-antimicrobial composites generation *Nanomaterials* **7** 1–18
[17] Rivero R, Molina M A, Rivarola C R and Barbero C A 2014 Pressure and microwave sensors/actuators based on smart hydrogel/conductive polymer nanocomposite *Sensors & Actuators B: Chemical* **190** 270–8
[18] Chaudhary V, Thakur A K and Bhowmick A K 2011 Improved optical and electrical response in metal-polymer nanocomposites for photovoltaic applications *J. Mater. Sci.* **46** 6096–105
[19] Gautama A and Ramb S 2010 Preparation and thermomechanical Properties of Ag-PVA Nanocomposite Films *Mater. Chem. Phys.* **119** 266–71
[20] Zhang J and Peppas N A 2000 Synthesis and characterization of pH- and temperature-sensitive poly(methacrylic acid)/poly(N-isopropylacrylamide) interpenetrating polymeric networks *Macromolecules* **33** 102–7
[21] Le Ouay B and Stellacci F 2015 Antibacterial activity of silver nanoparticles: a surface science insight *Nanotoday* **10** 339–54
[22] Prabhu S and Poulose E K 2012 Silver nanoparticles: mechanism of antimicrobial action, synthesis, medical applications, and toxicity effects *International Nano Letters* **2** 32
[23] Chen D, Qiao X, Qiu X and Chen J 2009 Synthesis and electrical properties of uniform silver nanoparticles for electronic applications *J. Mater. Sci.* **44** 1076–81
[24] Tsuboi A, Nakamura K and Kobayashi N 2016 Chromatic control of multicolor electrochromic device with localized surface plasmon resonance of silver nanoparticles by voltage-step method *Sol. Energy Mater. Sol. Cells* **145** 16–25
[25] Xiang Y and Chen D 2007 Preparation of a novel pH-responsive silver nanoparticle/poly(HEMA–PEGMA–MAA) composite hydrogel *Eur. Polym. J.* **43** 4178–87
[26] Monerris M, Broglia M, Yslas I, Barbero C and Rivarola C 2017 Antibacterial scaffolds nanocomposites synthesized by *in situ* photochemical formation of Ag nanoparticles inside biocompatible hydrogels *Express Polymer Letters* **11** 946–62
[27] Rivero R E, Alustiza F, Rodríguez N, Bosch P, Miras M C, Rivarola C R and Barbero C A 2015 Anisotropic mechanical behavior of macroporous biocompatible hydrogels: physicochemical and mechanical characterization *Reactive and Functional Polymers* **97** 77–85
[28] Rivero R, Alustiza F, Capella V, Liaudat C, Rodriguez N, Bosch P, Barbero C and Rivarola C 2017 Physicochemical properties of ionic and non-ionic biocompatible hydrogels in water and cell culture conditions: relation with type of morphologies of bovine fetal fibroblasts in contact with the surfaces *Colloids and Surfaces B: Biointerfaces* **158** 488–97
[29] Silverstein R M, Webster F X, Kiemle D J and Bryce D L 1981 *Spectrometric Identification of Organic Compounds* (New York: Wiley)
[30] Farooqi Z H, Butt Z, Begum R, Khan S R, Sharif A and Ahmed E 2015 Poly(N-isopropylacrylamide-co-methacrylic acid) microgel stabilized copper nanoparticles for catalytic reduction of nitrobenzene *Materials Science-Poland* **33** 627–34
[31] Nesic A, Panic V, Ostojic S, Micic D, Pajic-Lijakovic I, Onjia A and Velickovic S 2016 Physical-chemical behavior of novel copolymers composed of methacrylic acid and 2-acrylamido-2-methylpropane sulfonic acid *Mater. Chem. Phys.* **174** 156–63
[32] Durmaz S and Okay O 2000 Acrylamide/2-acrylamido-2-methylpropane sulfonic acidsodium salt-based hydrogels: synthesis and characterization *Polymer* **41** 3693–704
[33] Rivarola C R, Biasutti M A and Barbero C A 2009 A visible light photoinitiator system to produce acrylamide based smart hydrogels: Ru(bpy)$_3^{+2}$ as photopolymerization initiator and molecular probe of hydrogel microenvironments *Polymer* **50** 3145–52
[34] Ibarra-Montaño E L, Rodríguez-Laguna N, Sánchez-Hernández A and Rojas-Hernández A 2015 Determination of pKa values for acrylic, methacrylic and itaconic acids by ^{1}H and ^{13}C NMR in deuterated water *Journal of Applied Solution Chemistry and Modeling* **4** 7–18
[35] Tully P S Sulfonic Acids. 1997 ed Kroschwitz *Kirk-Othmer Encyclopedia of Chemical Technology* 4th Ed (New York: Wiley) Vol., p 194
[36] Schild H G 1992 Poly(N-isopropylacrylamide): experiment, theory and application *Prog. Polym. Sci.* **17** 163–249
[37] Molina M A, Rivarola C R and Barbero C A 2011 Effect of copolymerization and semi-interpenetration with conducting polyanilines on the physicochemical properties of poly(N-isopropylacrylamide) based thermosensitive hydrogels *Eur. Polym. J.* **47** 1977–84
[38] Peppas N, Bures P, Leobandung W and Ichikawa H 2000 Hydrogels in pharmaceutical formulations *European Journal Pharmaceutics Biopharmaceutics* **50** 27–46
[39] Molina M A, Rivarola C R and Barbero C A 2012 Study on partition and release of molecules in superabsorbent thermosensitive nanocomposites *Polymer* **53** 445–53
[40] Quintana J R, Valderruten N E and Katime I 1999 Synthesis and swelling kinetics of poly(dimethylaminoethyl acrylate methylchloride quaternary-co-itaconic acid) hydrogels *Langmuir* **15** 4728–30
[41] Karadağ E, Üzüm Ö B and Saraydin D 2005 Water uptake in chemically crosslinked poly (acrylamide-co-crotonic acid) hydrogels *Mater. Des.* **26** 265–70
[42] Masaro L and Zhu X X 1999 Physical models of diffusion for polymer solutions, gels and solids *Prog. Polym. Sci.* **24** 731–75
[43] Lees F P and Sarram P 1971 Diffusion coefficient of water in some organic liquids *Journal of Chemical & Engineering Data* **16** 41–4
[44] Krušić M K and Filipovic J 2006 Copolymer hydrogels based on N-isopropylacrylamide and itaconic acid *Polymer* **47** 148–55
[45] Nakamura T, Magara H, Herbani Y and Sato S 2011 Fabrication of silver nanoparticles by highly intense laser irradiation of aqueous solution *Applied Physics A* **104** 1021–4
[46] Alarcon E, Griffith M and Udekwu K 2015 Silver nanoparticle applications. in the fabrication and design of medical and biosensing devices ed N Pacioni, C Borsarelli, V Rey and A Veglia *Engineering Materials, Synthetic Routes for the Preparation of Silver Nanoparticles A Mechanistic Perspective* chapter 2 p. 13–46(Switzerland: Springer International Publishing)

[47] Zewde B, Ambaye A, Stubbs J III and Dharmara R A 2016 Review of Stabilized Silver Nanoparticles—Synthesis, Biological Properties, Characterization, and Potential Areas of Applications. JSM Nanotechnology *Nanomedicine* **4** 1043–57
[48] Bastús N G, Merkoçi F, Piella J and Puntes V 2014 Synthesis of highly monodisperse citrate-stabilized silver nanoparticles of up to 200 nm: kinetic control and catalytic properties *Chem. Mater.* **26** 2836–46
[49] López-Miranda A, López-Valdivieso A and Viramontes-Gamboa G 2012 Silver nanoparticles synthesis in aqueous solutions using sulfite as reducing agent and sodium dodecyl sulfate as stabilizer *Journal of Nanoparticle Research* **14** 1101